Large-scale erosion rates from in situ-produced cosmogenic nuclides in European river sediments

M. Schaller [a,*], F. von Blanckenburg [a], N. Hovius [b], P.W. Kubik [c]

[a] *Gruppe Isotopengeologie, Mineralogisch-Petrographisches Institut, Universität Bern, Erlachstrasse 9a, CH-3012 Bern, Switzerland*
[b] *Department of Earth Sciences, University of Cambridge, Downing Street, Cambridge CB2 3EQ, UK*
[c] *Paul Scherrer Institut, c/o Institute of Particle Physics, ETH Hönggerberg, CH-8093 Zürich, Switzerland*

Abstract

We have calculated long-term erosion rates of 20–100 mm/kyr from quartz-contained ^{10}Be in the bedload of middle European rivers for catchments ranging from 10^2 to 10^5 km^2. These rates average over 10–40 kyr and agree broadly with rock uplift, incision and exhumation rates, historic soil erosion rates, and erosion rates calculated from the measured sediment loads of the same rivers. Moreover, our new erosion rate estimates correlate well with lithology and relief. However, in the Regen, Neckar, Loire, and Meuse catchments, cosmogenic nuclide-derived erosion rates are consistently 1.5–4 times greater than the equivalent rates derived from measured river loads. This may be due to the systematic under-representation of high-magnitude, low-frequency transport events in the gauging records which cover less than a century. Alternatively the discrepancy may derive from spatially non-uniform erosion and preferential tapping of deeper sections of the irradiation profile. A third explanation relates the high cosmogenic nuclide-derived erosion rates to inheritance of an elevated Pleistocene erosion signal. Uncertainties associated with the cosmogenic nuclide-derived erosion rate estimates are not greater than the potential errors in conventional estimates. Therefore, the cosmogenic nuclide approach is an effective tool for rapid, catchment-wide assessment of time-integrated rates of bedrock weathering and erosion, and we anticipate its fruitful application to the Quaternary sedimentary record. © 2001 Elsevier Science B.V. All rights reserved.

Keywords: erosion; Be-10; cosmogenic elements; Europe

1. Introduction

Strong feedbacks exist between erosion and climate, tectonics, topography, soil production and land use. Understanding these feedbacks requires quantification of erosion through time, specifically at the catchment scale. Conventional techniques used to assess catchment-wide erosion rates convert suspended and dissolved loads of rivers into rates of downwearing of the landscape [1,2]. This method relies on river gauging records limited to the last hundred years or less. Such records do not normally contain rare (centennial or millennial) flood events which transport large volumes of sediment. Moreover, bedload transport com-

* Corresponding author. Fax: +41-31-631-49-88;
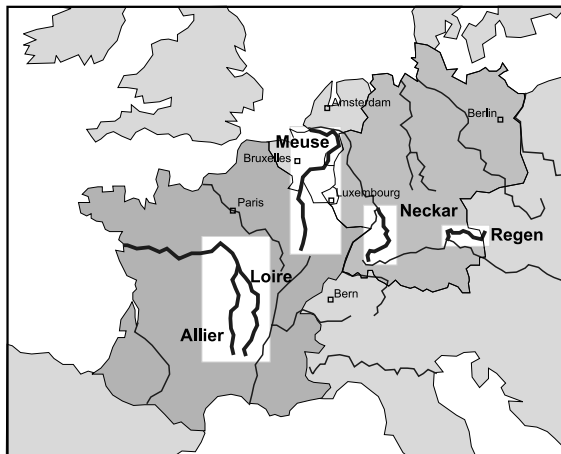E-mail: mirjam@mpi.unibe.ch

Fig. 1. Map of middle Europe showing the location of the Regen, Neckar, Meuse, and Loire catchments.

monly remains unrecorded. Rare estimates of long-term (1 kyr), catchment-wide erosion rates have been calculated from lake and reservoir fills (e.g. [3]), and from rock volumes removed from a landscape of known age and initial geometry (e.g. [4]). Recently developed techniques make use of geochemical mass balances of both dissolved and suspended river chemistry to calculate catchment-wide erosion rates [5,6].

Isotope geochemistry now offers an alternative approach to erosion estimates, exploiting the nuclides produced within mineral grains due to bombardment by secondary cosmic rays [7]. For example, the concentration of ^{10}Be in quartz at the Earth's surface is a function of the rate of erosion of the host rock [8]. This may be used to determine exposure ages and erosion rates of bedrock surfaces [9,10], and to constrain catchment-wide erosion rates from alluvial sediments [11–13]. The latter application makes use of the mixing of single bedrock surface samples by hillslope and fluvial processes. This application has been validated in small catchments (1–10 km^2), for example by comparing accumulation rates of alluvial fans with erosion rates derived from the cosmogenic isotope contents of sediments supplied by the corresponding hillside catchments [12].

In order to apply this approach to intermediate-size catchments (10^2–10^5 km^2), we have studied four rivers with well-constrained sus-

pended and dissolved loads. They are the Regen, Neckar, Meuse, and Loire rivers. These rivers drain middle European upland areas where the fluvial topography ensures continuous transport of sediment. Moreover, the middle European uplands have enjoyed relative tectonic stability during the Quaternary, and remained mostly free of ice throughout this period. The four rivers were selected to cover a range of catchment sizes and lithological complexity. Here, we present our results, and evaluate the complexities introduced into the cosmogenic approach by potential violations of the assumption of spatially and temporally uniform erosion upon which it is based.

2. Study areas and methodology

2.1. Study areas and sampling strategy

The Regen (SE Germany), Neckar (SW Germany), Meuse (NE France, Belgium, Netherlands) and Loire (central France) are all situated in the uplands of middle Europe (Fig. 1). Their headwaters are typically located between 1000 m and 1500 m a.s.l., in forested, fluvially dissected hills with mostly regolith-mantled slopes. The suspended and dissolved load of the upper Loire river has been analyzed by Grosbois et al. [14] and Négrel and Grosbois [15]. Tebbens [16] and Huisink [17] have studied extensively the evolution of the Meuse fluvial system and its sediment budget. At first order, climate and land use are homogeneous across middle Europe, with precipitation rates of 600–1500 mm/yr, and average annual temperatures of 7–11°C (Table 1), and differences in erosion rates between catchments are not expected to result from climatic forcing. By contrast, population density and lithology differ significantly between the four catchments. Whereas the Regen and Loire catchments are sparsely populated (1–100 persons/km^2), the Neckar and Meuse drainage areas support greater population densities (100–600 persons/km^2). The Loire catchment is dominated by agriculture while the Neckar region is largely forested. Of the four drainage basins, the Meuse is most urbanized. We expect

Table 1
Characteristics of drainage basins

		Regen	Neckar	Meuse	Loire/Allier
Drainage area	km^2	2911	14 447	31 645	42 637
Unit discharge	10^5 l/yr/km^2	4.51	3.48	2.88	2.95
Relief	km	1.13	0.93	0.69	1.89
Slope	m/km	13.6	5.6	1.6	3.6
Hypsometric integral[a]		0.25	0.41	0.31	0.27
Mean annual temperature[b]	°C	7	8	9	11
Mean annual rainfall in valleys[b]	mm/yr	600	700–800	700–800	600–700
Mean annual rainfall in mountains[b]	mm/yr	1400	1000	1100	1500
Population density[c]	p/km^2	1–100	100–600	100–600	10–100
Land use: agricultural land[c,d,e,f]	%	59	48	64	73
Land use: forest[c,d,e,f]	%	28	38	29	20
Land use: urbanized land[c,d,e,f]	%	13	14	7	7
Lithology		crystalline	sediments	sediments schists	crystalline sediments volcanics
Last glacial maximum glaciation[g,h,i,j]		cirque and minor valley glaciers	cirque and minor valley glaciers	no glaciation	ice caps
Quaternary tectonic uplift rate[k,l,m]	mm/kyr		100	60	75

[a] Loire hypsometry includes area upstream of Tours.
[b] Klimadiagramm-Weltatlas [41].
[c] World Atlas of Agriculture [42].
[d] Statistisches Landesamt Bayern.
[e] Statistisches Landesamt Baden-Württemberg.
[f] Centraal Bureau voor de Statistiek, The Netherlands.
[g] Hantke [43].
[h] Van den Berg [29].
[i] Rother [44].
[j] Veyret [45].
[k] Zippelt and Mälzer [46].
[l] Van den Berg [47].
[m] Veldkamp [48].

that land use and population density exert a complex control on modern sediment yields from all four catchments. A more permanent factor governing erosion is lithology. In order to assess the potential effect introduced by different source rock lithologies, we present data for two rivers in sedimentary rocks (Neckar and Meuse) and two catchments dominated by crystalline outcrops (Regen and Loire).

Within each catchment, sediment samples were collected at regular intervals along the trunk stream and on major tributaries, immediately upstream of their point of entry into the main river. Along the river Regen, samples were obtained every 20–30 km. Sampling intervals were 30–70 km in the other catchments. Samples were col-

lected during low flow from exposed sand bars in the active channel. Where no fresh sediment accumulations were present, an Eckman bedload sampler was used to obtain material from the submerged channel side. All samples consisted mainly of silt- to gravel-sized sediments.

2.2. Analytical techniques and data processing for cosmogenic nuclide-derived erosion rates

The bulk samples were separated into narrow grain size ranges (Table 2) and prepared for determination of the ^{10}Be concentration. For each sample, approximately 50 g of quartz was purified, followed by the simplified element separation method of von Blanckenburg et al. [18]. Acceler-

Table 2
Cosmogenic nuclide erosion rate data

Sample[a]	Drainage area (km²)	Altitude (m)	Latitude N	E	Mean altitude (m)	Mean latitude N	^{10}Be concentration (1)[b] (10^5 atoms/g(qtz))	Apparent age (kyr)	Erosion rate (mm/kyr)	Error (2)[c] (mm/kyr)	Total error (3)[d] (mm/kyr)
reg-5	2708	330	49° 08'	12° 07'	590	49°	2.31 ± 0.33	25.1	23.8	3.4	4.1
reg-7	2312	350	49° 11'	12° 24'	610	49°	2.44 ± 0.19	25.9	23.0	1.8	2.3
reg-11	389	380	49° 15'	12° 43'	520	49°	2.68 ± 0.21	31.0	19.2	1.5	2.0
reg-12A	1358	390	49° 11'	12° 44'	710	49°	2.45 ± 0.24	24.0	24.8	2.4	2.9
reg-12	1358	390	49° 11'	12° 44'	710	49°	2.45 ± 0.17	24.1	24.7	1.7	2.3
reg-12D	1358	390	49° 11'	12° 44'	710	49°	2.54 ± 0.16	25.0	23.8	4.3	5.5
reg-13	229	400	49° 14'	12° 50'	720	49°	2.37 ± 0.17	23.0	25.9	1.8	2.5
reg-14	1010	410	49° 08'	12° 50'	720	49°	2.93 ± 0.21	28.3	20.8	1.5	2.0
reg-18A	156	600	49° 03'	13° 12'	890	49°	2.69 ± 0.52	22.7	25.9	5.0	5.9
reg-18	156	600	49° 03'	13° 12'	890	49°	2.62 ± 0.21	22.1	26.7	2.1	2.8
reg-18D	156	600	49° 03'	13° 12'	890	49°	2.36 ± 0.23	19.9	29.7	2.9	3.5
reg-19	107	590	49° 02'	13° 16'	890	49°	2.91 ± 0.23	24.5	24.0	1.9	2.5
reg-19	107	590	49° 02'	13° 16'	890	49°	2.91 ± 0.22	24.5	23.9	1.8	2.4
reg-20	290	570	49° 01'	13° 13'	870	49°	2.49 ± 0.18	21.3	27.7	2.0	2.6
neck-1	422	600	48° 08'	8° 37'	700	48°	1.33 ± 0.12	13.1	46.6	4.2	5.3
neck-2	850	430	48° 24'	8° 40'	680	48°	0.71 ± 0.09	7.2	86.5	11.1	13.0
neck-3	3392	250	48° 45'	9° 24'	570	48°	0.63 ± 0.09	6.9	91.0	12.8	14.9
neck-4	3392	250	48° 45'	9° 24'	570	48°	0.70 ± 0.07	7.7	81.2	8.2	9.8
neck-5	13602	130	49° 25'	8° 53'	450	49°	0.65 ± 0.07	8.0	79.9	8.3	9.7
neck-6	13095	130	49° 28'	8° 28'	450	49°	0.75 ± 0.07	9.2	68.9	6.1	7.4
neck-6	13095	130	49° 28'	8° 28'	450	49°	0.59 ± 0.06	7.3	87.8	9.4	10.8
neck-6D	13095	130	49° 28'	8° 28'	450	49°	0.89 ± 0.01	10.9	58.0	7.9	9.2
neck-7	12761	150	49° 18'	9° 08'	460	49°	0.56 ± 0.07	6.8	94.4	11.6	13.3
neck-7	12761	150	49° 18'	9° 12'	460	49°	0.52 ± 0.08	6.3	101	15	17
neck-8	5851	185	49° 00'	9° 12'	510	49°	0.49 ± 0.05	5.7	112	12	14
neck-10	298	290	48° 51'	8° 38'	710	49°	1.44 ± 0.18	14.1	43.3	5.5	6.5
meu-1	904	280	48° 23'	5° 42'	370	48°	2.12 ± 0.15	28.0	21.7	1.5	2.0
meu-4	3775	158	49° 36'	5° 04'	320	49°	3.04 ± 0.27	42.1	14.1	1.3	1.6
meu-7	9293	120	50° 00'	4° 43'	300	49°	2.52 ± 0.25	35.4	17.0	1.7	2.1
meu-9	12267	95	50° 19'	4° 54'	300	49°	1.54 ± 0.14	21.7	28.6	2.5	3.0
meu-10	15121	90	50° 26'	5° 00'	280	50°	1.96 ± 0.30	28.0	21.9	3.4	4.0
meu-13A	21293	30	51° 02'	5° 46'	280	50°	2.35 ± 0.35	33.6	18.0	2.7	3.2
meu-13	21293	30	51° 02'	5° 46'	280	50°	1.65 ± 0.20	23.5	26.3	3.2	3.6
meu-13D	21293	30	51° 02'	5° 46'	280	50°	7.86 ± 0.11	11.2	57.1	8.2	9.8
meu-14	25172	18	51° 17'	6° 02'	270	51°	1.42 ± 0.11	20.5	30.5	2.4	2.9
meu-15C	25720	14	51° 30'	6° 10'	260	51°	0.74 ± 0.08	10.7	60.2	6.2	7.1
meu-15C	25720	14	51° 30'	6° 10'	260	51°	0.97 ± 0.09	14.1	45.2	4.2	5.0

Table 2 (continued)

Sample[a]	Drainage area (km²)	Altitude (m)	Latitude N	E	Mean altitude (m)	Mean latitude N	^{10}Be concentration (1)[b] (10⁵ atoms/ g(qtz))	Apparent age (kyr)	Erosion rate (mm/kyr)	Error (2)[c] (mm/kyr)	Total error (3)[d] (mm/kyr)
loi-2	42 133	55	47° 26'	0° 59'	480	46°	1.39 ± 0.16	16.9	36.6	4.1	4.9
loi-2	42 133	55	47° 26'	0° 59'	480	46°	1.40 ± 0.18	16.9	36.6	4.7	5.5
loi-7	37 390	100	47° 53'	2° 00'	530	46°	1.76 ± 0.18	20.4	29.9	3.1	3.7
loi-10	32 994	170	47° 00'	3° 04'	570	46°	1.76 ± 0.21	19.7	30.9	3.7	4.5
loi-11	18 420	175	46° 59'	3° 09'	500	46°	2.01 ± 0.42	21.3	28.7	4.5	5.3
loi-12	14 553	175	46° 57'	3° 04'	660	46°	1.57 ± 0.19	16.3	37.4	4.6	5.5
loi-12	14 553	175	46° 57'	3° 04'	660	46°	1.46 ± 0.17	15.2	40.4	4.8	5.7
loi-14A	13 531	195	46° 39'	3° 14'	690	46°	1.44 ± 0.17	14.6	41.9	4.8	5.8
loi-14	13 531	195	46° 39'	3° 14'	690	46°	1.62 ± 0.21	16.4	37.1	4.8	5.8
loi-15	12 830	225	46° 24'	3° 19'	720	46°	1.33 ± 0.15	13.2	46.4	5.2	6.4
loi-17	9 023	260	46° 04'	3° 28'	790	45°	1.55 ± 0.11	14.6	41.7	3.0	4.2
loi-18	1 582	280	45° 57'	3° 27'	730	46°	1.62 ± 0.14	15.9	38.3	3.3	4.2
loi-19	6 242	280	45° 55'	3° 22'	860	45°	1.17 ± 0.13	10.4	58.6	6.6	8.1
loi-21	750	440	45° 41'	3° 37'	850	46°	2.15 ± 0.26	19.0	31.4	3.8	4.5
loi-23	3 997	395	45° 28'	3° 17'	950	45°	1.55 ± 0.13	12.8	47.1	3.9	5.2
loi-25A	1 866	490	45° 07'	3° 29'	1100	45°	1.78 ± 0.20	13.0	45.8	5.2	6.4
loi-25	1 866	490	45° 07'	3° 29'	1100	45°	1.65 ± 0.17	12.1	49.4	5.1	6.3
loi-29	152	470	45° 08'	3° 26'	930	45°	1.65 ± 0.19	13.8	43.7	5.0	5.8
loi-32	5	950	45° 04'	3° 18'	950	45°	2.36 ± 0.22	19.4	30.5	2.8	3.5
loi-33	10	1150	44° 56'	3° 23'	1150	45°	2.54 ± 0.25	17.7	33.1	3.3	4.2
loi-34	10	1150	45° 00'	3° 24'	1150	45°	3.37 ± 0.26	23.6	24.6	1.9	2.6
loi-36	182	900	44° 44'	3° 51'	1130	45°	2.45 ± 0.26	17.4	33.8	3.5	4.4
loi-37	410	775	44° 53'	3° 55'	1170	45°	1.20 ± 0.15	8.3	72.2	8.9	10.7
loi-39	4 903	325	45° 45'	4° 12'	840	45°	1.09 ± 0.12	9.8	62.4	7.0	8.5
loi-40	6 501	280	46° 00'	4° 03'	780	45°	1.37 ± 0.16	12.9	47.4	5.5	6.5
loi-41	12 731	230	46° 30'	3° 54'	590	46°	2.15 ± 0.21	23.7	25.5	2.5	3.1
loi-45	1 323	65	47° 30'	1° 16'	110	48°	1.94 ± 0.16	32.7	19.0	1.6	2.0
loi-48	191	205	47° 08'	3° 12'	280	47°	7.00 ± 0.39	101.6	5.42	0.30	0.52
loi-49	380	185	47° 02'	3° 13'	290	47°	3.81 ± 0.23	54.8	10.7	0.7	1.0
loi-50	1 415	190	46° 50'	3° 30'	290	47°	2.42 ± 0.15	34.6	17.5	1.1	1.6
loi-51	376	195	46° 47'	3° 27'	240	47°	3.85 ± 0.28	57.6	10.2	0.7	1.0
loi-52	736	215	46° 31'	3° 41'	470	47°	2.15 ± 0.15	26.0	23.3	1.6	2.2
loi-54	2 551	232	46° 30'	4° 00'	410	46°	2.78 ± 0.21	36.0	16.6	1.3	1.7
loi-55	2 765	237	46° 21'	2° 19'	620	46°	1.89 ± 0.16	20.3	29.8	2.5	3.3
loi-56	150	320	46° 00'	2° 18'	390	46°	2.43 ± 0.21	32.1	18.8	1.6	2.2

[a] A = grain size 1–2 mm, C = grain size 0.25–0.5 mm, D = grain size 0.125–0.25 mm, no letter = grain size 0.5–1 mm.
[b] ^{10}Be concentration with analytical error.
[c] For inter-sample comparison: combined analytical, altitude (5%) and scaling factor error.
[d] For inter-method comparison: combined analytical, altitude (5%), scaling factor and production rate error.

ator mass spectrometry (AMS) was carried out at the PSI/ETH facility in Zürich and the measured [10]Be/Be ratios were corrected as described in Kubik et al. [19]. The calculated [10]Be concentrations and the corresponding analytical errors are listed in Table 2.

To calculate the erosion rates and apparent exposure ages of Table 2, the [10]Be production rate of Kubik et al. [19] has been used in a modified form (for details see Appendix 1 in the **EPSL Online Background Dataset**[1]). The new spallation production rate is 5.22 ± 0.22 atoms/g(qtz)/yr. An accurate representation of both stopped and fast muon contributions is important in erosion rate studies, where material is exhumed from great depth. For the muon surface production rates we have used 0.12 atoms/g(qtz)/yr for stopped muons and 0.027 atoms/g(qtz)/yr for fast muons [20]. Including muons, this results in a total surface production rate at sea level and high latitude (SLHL) for [10]Be of 5.37 ± 0.22 atoms/g(qtz)/yr.

For each sample listed in Table 2, the local surface production rates due to nucleons and due to muons were calculated by separately scaling the respective SLHL production rates to the mean altitude of the upstream catchment area (see text below for reasoning).

For the calculation of the [10]Be production below the surface, the nucleonic and the muonic components are again treated separately. For the nucleonic production below the surface the depth dependence of Masarik and Reedy has been used [21]. A zenith angle dependence similar to that in the atmosphere [22] has been taken into account. The depth dependences of the stopped and the fast muons have been extracted from Heisinger [20].

To be able to express the relation of measured concentration to the steady-state erosion rate in the conventionally used exponential format [8], the complex depth dependences of both the nucleonic and the muonic components were developed up to a depth of about 400 m into a series of exponential functions. For each production mechanism, a series of four exponential functions were sufficient to reproduce the depth dependence of the total production down to any depth to better than 1%. This complexity of four exponential production terms is regarded as necessary in the case of nucleons to adequately describe surface interface effects [21] and the zenith angle dependence [22]. In the case of muons, inclusion of the fourth small exponential term is required to accurately describe the production at great depth. The measured concentration can then be converted into erosion rates with the following equation:

$$C = P_{\mathrm{Nuc}}(0) * \sum_{i=1}^{4} \frac{a_i}{\left(\lambda + \dfrac{\rho * E}{b_i}\right)} + P_{\mu\mathrm{stopped}}(0) *$$

$$\sum_{j=1}^{4} \frac{a_j}{\left(\lambda + \dfrac{\rho * E}{b_j}\right)} + P_{\mu\mathrm{fast}}(0) * \sum_{k=1}^{4} \frac{a_k}{\left(\lambda + \dfrac{\rho * E}{b_k}\right)}$$

(1)

Here, E (cm/yr) is the erosion rate, λ (/yr) is the decay constant, ρ is the rock density (g/cm^3), and $P_{\mathrm{Nuc}}(0)$, $P_{\mu\mathrm{stopped}}(0)$ and $P_{\mu\mathrm{fast}}(0)$ are the local surface production rates of cosmogenic nuclides by spallation, stopped and fast muons, respectively. $a_{i,j,k}$ (dimensionless) and $b_{i,j,k}$ (g/cm^2) are the coefficients for the depth scaling of the production rates (Table 3). The $b_{i,j,k}$ should not be thought of as real physical 1/e attenuation lengths or mean absorption paths but only as parameters in the development of the complex depth functions into an exponential format.

It might be expected that inappropriate production rate altitude scaling in terrains with considerable relief and spatially variable erosion rates introduces a potentially large bias in catchment-wide erosion rate estimates. However, if a trunk stream consists of sediment from several tributaries with individual production rate P_k and area A_k and the flux of sediment F_k is at steady state with the erosion rate E_k, then it can be demonstrated that the concentration of cosmogenic nuclides in the trunk stream from each of the production mechanisms explored above, and ignoring

---

[1] http://www.elsevier.nl/locate/epsl; mirror site: http://www.elsevier.com/locate/epsl

Table 3

Coefficients for the development of the depth dependence of production rates into a series of exponential functions

Index	Production mechanism	a	b
			g/cm^2
$i=1$	nucleons	0.0491	0.003
$i=2$	$P_0 = 5.22$	−0.1264	3.221
$i=3$	atoms/g(qtz)/yr	0.3494	81.34
$i=4$		0.7275	140.22
$j=1$	stopped muons	0.4050	900
$j=2$	$P_0 = 0.12$	0.5240	1 330
$j=3$	atoms/g(qtz)/yr	0.0820	4 000
$j=4$		0.0020	14 000
$k=1$	fast muons	−0.3566	870
$k=2$	$P_0 = 0.027$	0.8619	1 668
$k=3$	atoms/g(qtz)/yr	0.4136	6 931
$k=4$		0.0791	24 500

radioactive decay, equals:

$$C = \frac{F_{10_{Betot}}}{F_{tot}} = \frac{\sum_{k=1}^{n} \frac{P_k^* A_k^* \Lambda}{\rho}}{E_{tot} * A_{tot}} \quad (2)$$

ρ is the rock density (g/cm^3), Λ (g/cm^2) is an absorption mean free path, and P_k (atoms/g(qtz)/yr) is the respective local surface production rates of the cosmogenic nuclide. F_{tot} is the total flux of sediment, $F_{10_{Betot}}$ is the cosmogenic nuclide flux leaving the system, E_{tot} is the total catchment's spatially averaged erosion rate and n is the number of tributaries. At steady state ^{10}Be leaving the system equals that produced by cosmogenic irradiation. Therefore, if P_k can be determined accurately for the entire catchment area the total concentration of ^{10}Be is independent of the differences in the tributary's erosion rate E_k.

The production rates of samples measured in this study have been determined for the mean upstream catchment altitudes, which were estimated for each sample with a 30′ digital elevation model. The mean altitudes used in this study should be accurate to within 5%.

Table 2 lists the calculated erosion rates with associated errors. Error (1) is the analytical uncertainty of the measured nuclide concentration (AMS counting statistics and standard correction, blank correction). Error (2) for the erosion rate includes an uncertainty for $P(0)$ based on the 5% uncertainty for the estimate of the mean alti-

tude of the upstream catchment area, and an uncertainty determined from the difference of the used Lal scaling to the recently published scaling algorithm of Dunai [23]. Error (3) for the erosion rate includes also an uncertainty for the SLHL production rate by nucleons. Error (3) is appropriate for inter-method comparisons, while error (2) is sufficient for inter-sample comparison.

The following parameters influence the erosion rate estimates, but have not been corrected for because either they amount to corrections far smaller than analytical uncertainties, or they are difficult to quantify exactly in catchments of the investigated sizes. The error on the surface production of ^{10}Be by stopped and fast muons could not be quantified. Also for the depth dependence of both production mechanisms no error has been determined. The latter uncertainty should, however, be small, as the depth dependences are based on a vast amount of experimental data. However, one can estimate the effect that different SLHL muon production rates would have on the erosion rates. A 50% increase in both muon $P(0)$ SLHL results in a 17% increase in erosion rate, while a 100% increase in both muon $P(0)$ increases the erosion rate by 34%. The influence of a varying geomagnetic field intensity through time on the cosmogenic nuclide production rate is negligible at latitudes of the study areas [24,25]. Decreasing cosmic ray flux intensity due to the dip angle of the irradiated surface in a catchment with a mean
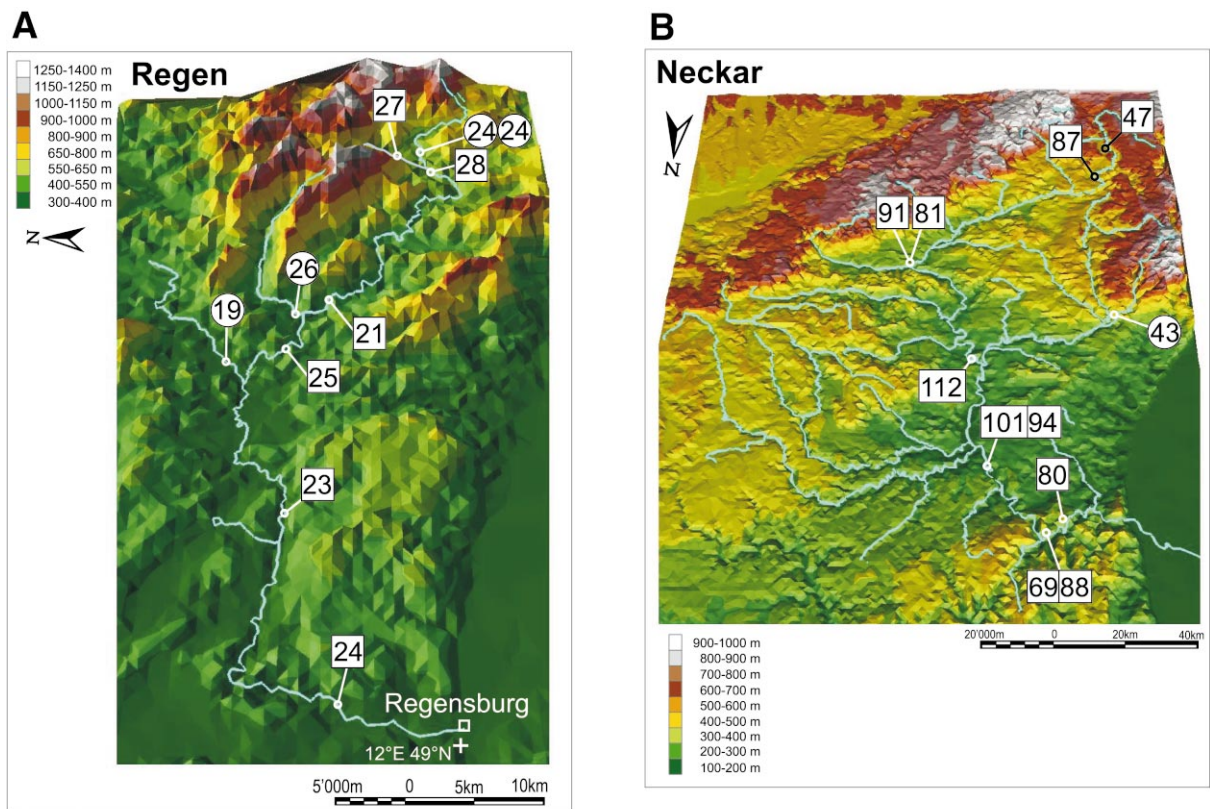
Fig. 2. (A–D) Sample locations and erosion rate estimates (in mm/kyr) calculated from cosmogenic [10]Be in quartz for the Regen, Neckar, Meuse, and Loire catchments. Samples with a grain size range of 0.5–1 mm taken from main streams are shown as squares; samples taken on tributaries are shown as circles.

slope of 10° leads to a reduction of the production rate of less than 1% [19]. Furthermore, corrections of shielding by snow or vegetational cover are negligible based on the production rate profile of Masarik and Reedy [21]. The selective dissolution of regolith, and the consequent relative enrichment of quartz, should be addressed in basin-averaged erosion rate studies [26]. As the analyzed catchments contain a great variety of lithologies and regolith thicknesses no generally applicable correction factor can be determined. For a sub-catchment dominated by granites, where a regolith thickness of 1 m and a quartz enrichment of two from bedrock to regolith is assumed, the corrected erosion rate is 40% higher than the uncorrected one. For a catchment containing also sandstones where no regolith dissolution is expected, this correction would be an overestimate. There-

fore, all reported erosion rates are not corrected for regolith dissolution and are minimum erosion rates. Density is strongly related to lithology and therefore not exactly determinable in medium-scaled catchments. The overall used density of 2.7 g/cm^3 for granites instead of 2.2 g/cm^3, which would be appropriate for sediments, again results in a minimum erosion rate. This does not affect the comparison between methods, as both river load gauging erosion rates and cosmogenic nuclide-derived erosion rates make use of the same density.

Special attention has to be paid to loess mixed into the regolith by solifluction. Late Pleistocene loess is abundant in some of the studied catchments, mainly the Neckar and Meuse [27]. This wind-blown component is not represented in the grain size fractions analyzed in this study. As a
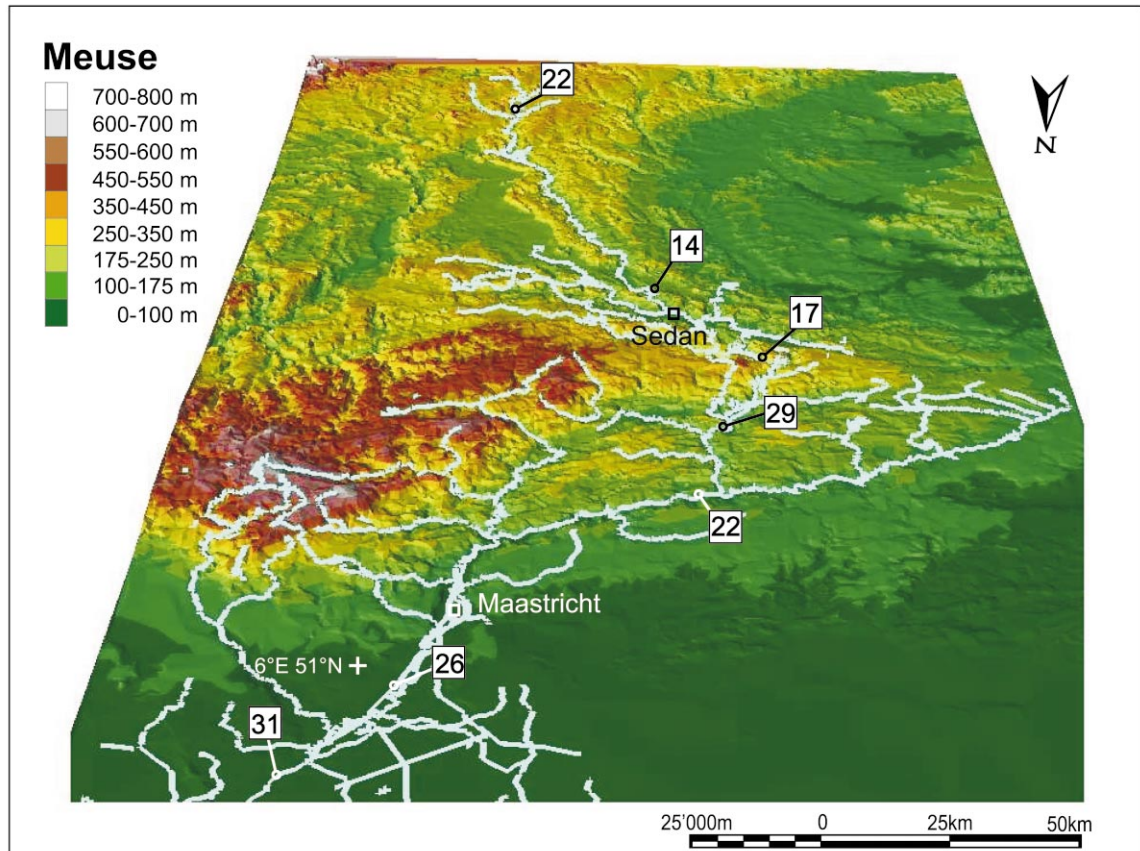
Fig. 2 (*continued*).

result, late addition of loess would not affect the cosmogenic results. Therefore, in easily erodible loess areas, cosmogenic nuclide-derived erosion rates will reflect the erosion before loess deposition, even if the actual erosion is much higher at present. In contrast, if loess has been admixed to the regolith before the onset of the erosion interval detected by cosmogenic nuclides (e.g. several 10 kyr), the nuclide concentration will have adjusted to the loess-dominated erodibility and corresponding erosion rates will reveal the actual erosion rate of the mixture. This is because the admixture of loess influences the cosmogenic nuclide-derived erosion rate indirectly by providing additional shielding from cosmic rays.

2.3. Estimation of river load gauging-derived erosion rates

The combined solid and solute load of a river can be used to calculate a catchment-wide erosion rate. The used loads have been obtained from the river authorities of the regions under investigation. Because in Section 4.2 we present a detailed comparison between methods it is important to analyze all sources of uncertainty carefully. The procedures for correction for anthropogenic and atmospheric contributions are detailed in Appendix 2 in the **EPSL Online Background Dataset**[1]. River loads and derived erosion rates are presented in Table 4.
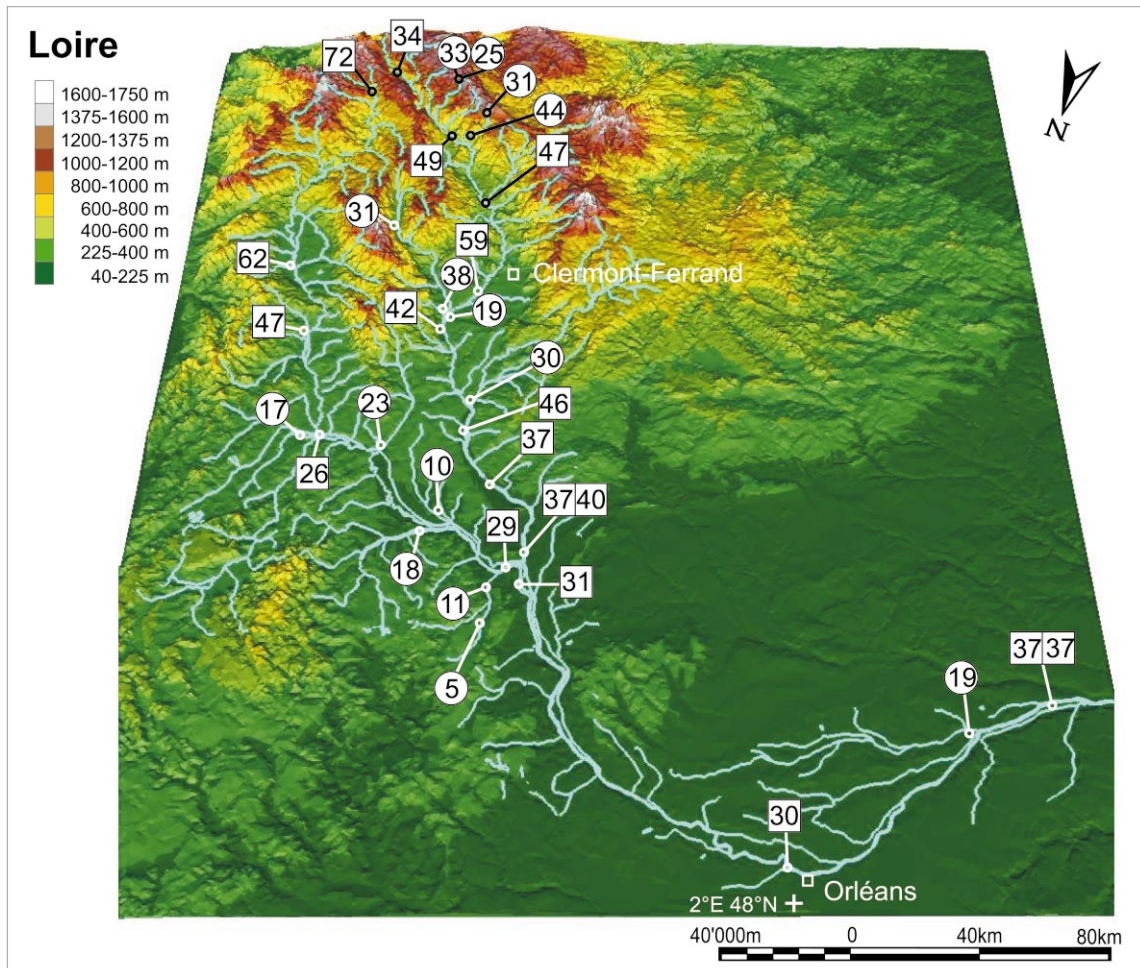
Fig. 2 (*continued*).

3. Results

3.1. Cosmogenic nuclide-derived erosion rates

Erosion rate estimates based on cosmogenic nuclide analyses (E_C) are presented in Fig. 2. The principal observations are as follows. In the Regen catchment, E_C ranges from 19 to 28 mm/kyr. The highest values were observed in the headwaters of the catchment, the lowest on a tributary with relatively subdued local relief. Where several grain size classes of a sample were analyzed, no

resolvable differences were found between apparent erosion rates.

A more heterogeneous erosion pattern emerged in the Neckar catchment. There, apparent erosion rates vary between $E_C = 47$ mm/kyr and $E_C = 112$ mm/kyr. The lowest rates were found in the sandstone-dominated uppermost part of the catchment: one tributary, entirely in sandstone, has an estimated erosion rate of $E_C = 43$ mm/kyr. Parts of the catchment with predominantly carbonaceous or evaporitic substrates have significantly higher apparent erosion rates. Several locks have trapped sediment along the Neckar in recent dec-

Table 4
River load gauging data

River	Station	Area km²	Discharge[a] m³/s	TDS[b] mg/l	TDS p[c] mg/l	TDS gw[d] mg/l	TSS[e] mg/l	TSS cor[f] mg/l	Total[g] mg/l	Total E[h] mm/kyr	E min[i] mm/kyr	E max[j] mm/kyr
Regen (I)	Regenstauf	2658	38	43	28	14	23	25	39	7	4	10
Neckar (II)	Deizisau	4010	50	563	284	142	29	32	174	25	24	83
	Poppenweiler	5005	61	588	299	150	36	40	189	27	24	86
	Lauffen	7916	88	549	281	141	33	36	177	23	20	72
	Rockenau	12676	139	695	333	167	42	46	213	27	23	93
	Mannheim	13966	154	608	303	152	47	51	203	26	24	80
Meuse (III)	Tailfer	12484	178	312	162	81	24	26	107	18	17	57
	Namêche	15328	191	376	186	93	29	32	125	18	16	54
	Liège	21254	257	369	182	91	26	29	120	17	14	52
	Eijsden	21649	261	362	179	90	26	29	118	17	14	51
	Heusden	32711	300	388	186	93	24	26	119	13	10	40
	Keizersveer	33580	306	372	181	91	15	17	107	11	7	34
Loire (IV)	Goudet	432	4	69	39	20	5	6	25	3	1	6
	Bas	3234	37	107	55	28	9	10	37	5	3	11
	Feurs	4960	42	170	83	42	11	12	53	5	3	14
	Villerest	6584	61	146	73	37	5	5	42	4	2	12
	Decize	16519	121	159	81	41	18	20	60	5	3	12
	Nevers	18208	171	160	83	42	22	24	65	7	4	16
	Gien	35500	394	190	99	50	27	30	80	10	6	23
	Orléans	36966	307	185	96	48	34	37	85	8	5	17
	Chaumont	40600	380	207	108	54	32	35	89	10	5	20
Allier (IV)	Langogne	324	7	31	18	9	3	3	12	3	2	7
	Langeac	1781	36	47	23	12	5	5	17	4	2	8
	Châtel	12430	112	165	85	43	17	19	61	6	3	13
	Villeneuve	13348	133	181	94	47	20	22	69	8	4	16
	Cuffy	14320	136	181	94	47	25	28	75	8	4	16

(I) Bayerisches Landesamt für Wasserwirtschaft.
(II) Bundesanstalt für Gewässerschutz Koblenz.
(III) RIWA (Vereniging van Rivierwaterbedrijven).
(IV) Agence de l'eau Loire-Bretagne.
[a] Mean annual discharge calculated from the data set as given by I, II, III and IV.
[b] Total dissolved solids.
[c] TDS corrected for precipitation and atmospheric input after Summerfield [49] and anthropogenic input after Berner and Berner [50].
[d] Pollution-corrected TDS corrected for groundwater influence after method described in Kille [51].
[e] Total suspended solids.
[f] TSS corrected for bed load [49], river inhomogeneity and organic material [52].
[g] Sum of TDS gw and TSS cor.
[h] Erosion rate calculated with a density of 2.7 g/cm³.
[i] Minimum erosion rate, for further explanations see Appendix 2 in the **EPSL Online Background Dataset**[1].
[j] Maximum erosion rate, for further explanations see Appendix 2 in the **EPSL Online Background Dataset**[1].

ades, and this has resulted in poor downstream mixing of the solid load. Local lithological controls on erosion rate therefore are reflected more in the Neckar data set than in results in less compartmentalized systems.

In the Meuse catchment, erosion rate estimates for the grain size 0.5–1.0 mm range from $E_C = 14$ mm/kyr to $E_C = 31$ mm/kyr, the highest rates being confined downstream of the Ardennes mountains. Smaller grain sizes yielded higher erosion rates (up to 60 mm/kyr) for the river section downstream of this upland area. This is attributed to admixture of Tertiary sands (grain size < 0.5 mm) from the channel base in the Roer Graben area. These sands have been shielded from irradiation since their deposition in the Late Tertiary and cosmogenic ^{10}Be has radioactively decayed. Samples thus affected are excluded from the discussion.

Cosmogenic nuclide-derived estimates of erosion rates in the Loire catchment decrease steadily along the trunk stream, from $E_C = 72$ mm/kyr in the headwaters to $E_C = 29$ mm/kyr at the confluence with the Allier. This decrease is caused by admixture of material with a high ^{10}Be concentration from tributaries draining areas with subdued erosion rates of $E_C = 5$ mm/kyr to $E_C = 23$ mm/kyr. In the drainage basin of the Allier, apparent erosion rates were more uniform, with values ranging from $E_C = 31$ mm/kyr to $E_C = 59$ mm/kyr. In contrast to the Tertiary sand deposits of the Meuse catchment, the sand-rich formations from the Tertiary in the Limagne Graben have been lithified and are subjected to weathering and surface erosion processes as all other rock formations are.

Cosmogenic nuclides yield estimates of the average erosion rate over the time the sampled material resided in the shallow subsurface, within one absorption depth length ($\sim$60 cm [8]). This residence time varies widely between and within the four catchments: Regen 20–30 kyr; Neckar 5–15 kyr; Meuse 20–40 kyr; and Loire and Allier 10–20 kyr.

3.2. River load gauging-derived erosion rates

The corrected total load of the river Regen re-sults in gauging-derived erosion rates (E_G) of 7 mm/kyr (Table 4). In the Neckar catchment, values for E_G for individual gauging stations are around 25 mm/kyr. It is worth noting that the solute load of the Neckar River is greater than its solid load, due to the abundance of carbonates and evaporites in the catchment. Stations along the Meuse display a downstream decrease of E_G from 18 mm/kyr at Tailfer to 11 mm/kyr at Keizersveer. In the Loire catchment we have found an apparent downstream increase of the solid load. This may be due in part to the low frequency of river gauging in that catchment (loads are recorded at monthly intervals). As a consequence, many short-lived, high-magnitude discharge and sediment transport events are not recorded by upstream stations. Because such events tend to diffuse downstream and concatenate with signals from other tributaries, records from downstream stations are more comprehensive, even at low sampling frequencies. The relatively strong increase in the total dissolved load is attributed to the transition from magmatic and metamorphic rocks upstream to mainly sedimentary rocks downstream. As a result of these trends, E_G varies from 3 mm/kyr at upstream gauging stations to 10 mm/kyr downstream.

The E_G for both catchments dominated by crystalline rocks, Regen and Loire, are 5–10 mm/kyr, and values for catchments in sedimentary rocks are higher by a factor of 3 (15–30 mm/kyr).

4. Discussion

4.1. General significance of erosion rate estimates

We believe that the measured cosmogenic nuclide concentrations faithfully record erosion rates at the time scale of the apparent exposure of the sampled material, that is 10–40 kyr (Table 2).

Firstly, our cosmogenic erosion rate estimates agree well with other, independent estimates. (1) Reported E_C and E_G values are of the same order. This coincidence is not necessarily expected, given the differences in techniques and sampled time scales. (2) Our E_C values are similar to Late Tertiary and Quaternary uplift rates of 60–70 mm/kyr
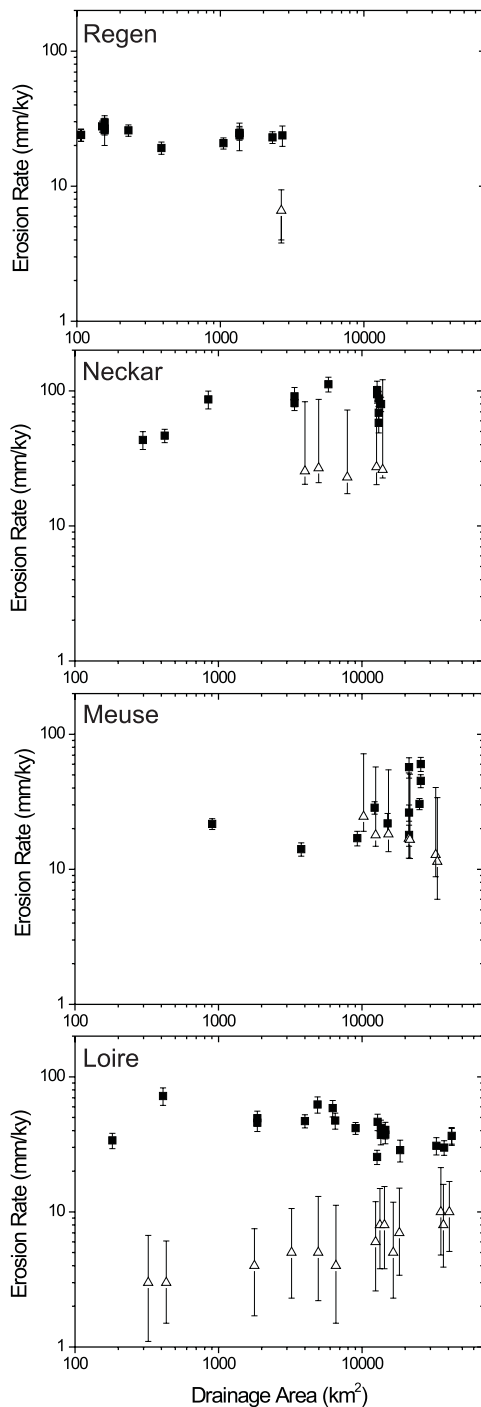
in the Massif Central and the Ardennes (Table 1). (3) They agree with average long-term (300 Myr) exhumation rates of 25–50 mm/kyr, estimated from Variscan rocks in the Regen area, Massif Central, and the Black Forest [28]. (4) Late glacial and Holocene erosion rates derived from sediment accumulation in a non-Alpine lake in the Massif Central range from 50 to 120 mm/kyr [3]. (5) Incision rates calculated from the elevation of Meuse river terraces of known age are 60 mm/kyr for the Quaternary [29]. Using the terrace stratigraphy of Larue [30] and of Pastre [31], incision rates of 70 and 90 mm/kyr have been calculated for the Allier basin for the last 0.6 Myr and 1 Myr, respectively. (6) Finally, Bork et al. [32] derived an erosion rate of 80 mm/kyr for the last 2 kyr from soil catena reconstructions in non-Alpine Germany.

Secondly, the high degree of uniformity of E_C within the Regen catchment, where differences in lithology and relief are small, demonstrates consistency and reproducibility of our estimates.

Thirdly, substantial downstream increases of the nuclide concentrations are not observed. This corroborates our assertion that further irradiation during sediment storage within the studied catchments is insignificant. Long-term ($\gg 10$ kyr) deposition of sediments and subsequent irradiation would result in a progressive downstream increase of cosmogenic nuclide dosage [12], and an associated decrease of apparent erosion rates.

Fourthly, in most samples, [10]Be concentrations are uniform across grain sizes (Table 3). This is to be expected where hillslope processes mobilize material across the spectrum of particle calibers.

←
Fig. 3. Cosmogenic nuclide-derived erosion rates (solid squares) and river load gauging-derived erosion rates (open triangles) plotted against drainage area upstream of sampling location. Errors of cosmogenic nuclide-derived erosion rates include uncertainties introduced by analytical errors, uncertainties in surface nucleonic production rates, an altitude uncertainty of 5% and a propagation of uncertainties in the atmospheric scaling of production rates. The error bars associated with river load gauging data represent minimal and maximal values (see Appendix 2 in the **EPSL Online Background Dataset**[1]). The cosmogenic nuclide-derived erosion rates are generally higher than river load gauging rates by a factor of 1.5–4.

Assuming that mass wasting introduces a dependence between cosmogenic nuclide concentration and grain size [11], we infer that hillslope transport processes in middle Europe are dominated by mechanisms such as slow creep and surface wash, and that landsliding does not play an important role. The latter process would preferentially produce large grains with low cosmogenic nuclide concentrations relative to the finer components of a random sediment sample [11].

The sum of this evidence gives us confidence that our E_C values are robust. We proceed to discuss the results in more detail based on this premise.

4.2. Comparison between methods

At any of our sample locations, E_C and E_G differ by a factor of 1.5–4 (Fig. 3). Even when we take into account all major uncertainties associated with river load gauging as discussed in Appendix 2 in the **EPSL Online Background Dataset**[1] (e.g. an addition of 30% to the total solid load representing the unmeasured bedload in catchments with a crystalline basement), the two methods yield distinctly different results, with the notable exception of the Meuse. Moreover, these differences cannot be explained fully by the uncertainties associated with our method for estimating erosion rates from cosmogenic nuclide concentrations (Section 2.2). Most appropriate corrections for potential biases in erosion rate estimates would further increase the discrepancy between results obtained by the two methods. For example, differential dissolution may cause a relative enrichment of quartz in long-lived regoliths. Quartz enrichment by a factor of two in a 1 m thick regolith, as commonly observed in middle Europe, would demand an upward correction of E_C by 40%. Another potential complication derives from the variation of quartz concentration in the substrate across a catchment. Because the weatherability and erodibility of bedrock tend to decrease with increasing quartz content [33], an overrepresentation of quartz-rich source rock in the river load would also demand an upward correction of E_C. A third cause of bias is the deposition of loess across some of middle Europe dur-

ing the Late Pleistocene [27]. As discussed in Section 2.2, the late addition of highly erodible loess would increase E_G, but does not affect our E_C estimates because they have been derived from coarser material only. The difference between E_G and E_C would be smaller in loess-rich areas than elsewhere: inflation of loess does not explain the observed discrepancy between E_G and E_C.

One reason for a downward adjustment of our E_C values would be the sudden vertical mixing of a regolith profile with a nuclide concentration that decreases with depth. This would result in a transient deficiency of nuclides at the surface [12]. The magnitude of this depletion for a typical middle European, 1 m thick regolith which was at steady state before mixing would be 40%. However, even if such mixing had occurred throughout our four catchments, the resulting 40% excess in E_C would not explain the up to four-fold excess of measured E_C over E_G.

Three principal explanations for the phenomenon remain.

1. *River load gauging and sampling time scales*: Part of the observed discrepancy may derive from the systematic underestimation of E_G [34]. River load measurements typically span between 10 and 100 years. At this time scale rare, but volumetrically important floods may not be captured. The cosmogenic nuclide method integrates over 10–40 kyr and does cover the entire spectrum of discharges and loads. Bork et al. [32] have illustrated the importance of high-magnitude, low-frequency erosion events in intensively farmed middle Europe: between 1961 and 1990, soil erosion rates were $\sim$80 mm/kyr; for the flood-rich year 1342 they calculated an erosion rate of 23 000 mm/kyr.

2. *Spatially non-uniform erosion*: The model assumption of surface erosion is violated by episodic spatially non-uniform erosion, and selective tapping of deeper segments of the irradiated substrate. Exhumation of material from depths with lower nuclide concentrations than at the undissected surface may lead to overestimation of E_C as compared to E_G. Linear dissection of the middle European land-

scape caused by rilling and gullying on agricultural plots [35] has been caused by changes in land use during historic times [32].

3. *Enhanced erosion during the Late Pleistocene*: The difference between E_C and E_G may be due in part to relatively high pre-Holocene erosion rates. A pre-Holocene erosion signal may have been inherited in two ways. (1) Following a change in erosion rate, time is required to achieve a new steady-state nuclide concentration. Thus, a transient time lag exists between the apparent nuclide erosion rate and the actual erosion rate [11,36]. For example, a step change from an erosion rate of 30 mm/kyr to no erosion at 10 kyr would result in an apparent maximum erosion rate today of 20 mm/kyr (Fig. 4). Vertical regolith mixing [12] would obscure the change in measured erosion rate even further. (2) Our samples may contain some re-entrained, pre-Holocene floodplain sediments, carrying a late glacial nuclide signal. Because this material has been irradiated since deposition, the pre-Holocene signal has been diluted: 10 kyr of irradiation at the surface of a terrace would cause a reduction of the apparent erosion rate by 25% (Fig. 4). If the storage time is short compared to the half-life of ^{10}Be, the reduction of the nuclide concentration due to radioactive decay is negligible. Both scenarios imply that an important component of the nuclide signal in our samples was produced under pre-Holocene conditions. In non-glaciated areas of middle Europe, the Late Glacial was characterized by enhanced mechanical weathering due to frequent freeze–thaw transitions, reduced biomass, and pervasive solifluction on hillslopes [37]. Some reported late glacial erosion rates were more than twice their Holocene equivalents [3].

Although there is abundant evidence of major increases in erosion rates due to anthropogenic activities [35], a surprising result of this study is that we observe the opposite. Taking the reported erosion estimates from river loads at face value, our nuclide-derived estimates of long-term erosion rates suggest that today's human impact on spatially averaged erosion is insignificant compared
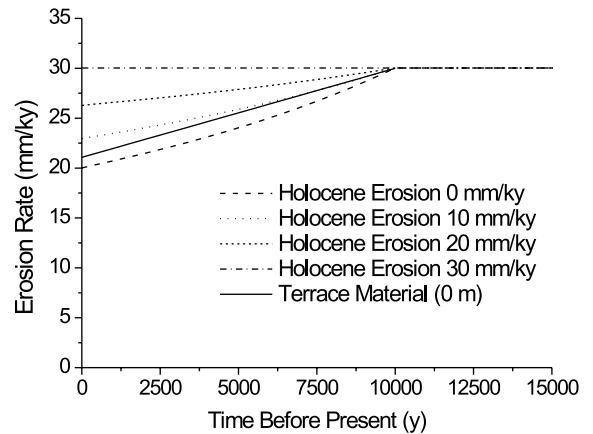

Fig. 4. Evolution of cosmogenic nuclide-derived erosion rates after a step change of erosion rate at 10 kyr from 30 mm/kyr to lower values of 20, 10 and 0 mm/kyr. The maximum possible decrease in erosion rate is 35%. The bold line represents an erosion rate calculated from re-irradiated and re-worked terrace material with a prior erosion rate history of 30 mm/kyr.

to the effect of climate change from Pleistocene to Holocene time.

Regardless of the actual cause of the inter-method discrepancy, we are dealing with a systematic effect that is likely to affect all catchments to the same extent.

4.3. Controls on erosion and weathering rates

Long-term erosion rates vary between the studied catchments by up to a factor of three. We briefly explore the possible causes of this variation.

Today's climate and land use do not differ significantly between the four catchments (Section 2.1, Table 1). Therefore, they can be excluded as governing controls on erosion rate. Lithology and relief remain as possible controls. The effect of lithology is evident from the elevated E_C values found in the Neckar catchment, which contains some easily abradable and dissolvable rock types (Table 4). Within the Neckar catchment, sample localities dominated by sandstones have lower E_C values than those in chemical sediments. The Regen, Loire, and Meuse (with the exception of its southernmost component which is located within the Paris Basin) catchments are situated in rock
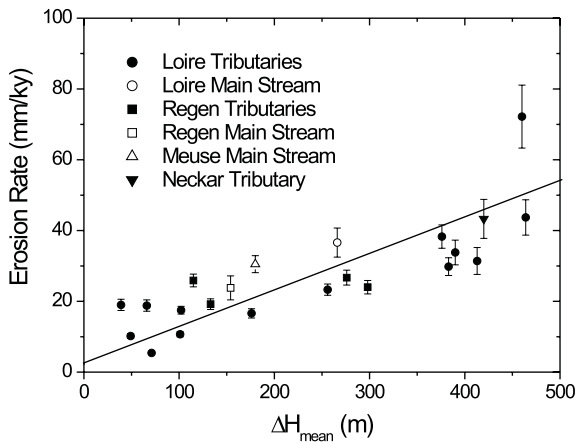
Fig. 5. Time-averaged, cosmogenic nuclide-derived erosion rate versus a relief parameter ΔH_{mean}. ΔH_{mean} is the mean altitude (from DEM) minus the minimum altitude of a catchment. This approach differs from the relief parameter used by Ahnert [39] (mean of maximum minus minimum altitude) because catchments in this study are too small to infer statistically meaningful mean reliefs. ΔH_{mean} of tributaries is based on their entire catchment's area. ΔH_{mean} for main streams is averaged over DEM models of several upstream subsegments. All rivers draining chemical sediments (Neckar, upstream Meuse) have been excluded. The linear regression yields a slope of 0.1 Myr^{-1}.

types of comparable erodibility and solubility. We propose, therefore, that differential dissolution has not been a major cause of the differences in E_C between and within these catchments. Instead, topography may be the dominant control on erosion rate (cf. [35,38]). This is confirmed (Fig. 5) by the clear, positive correlation between E_C and a measure of the relief, ΔH_{mean} (mean minus minimum altitude of the catchment area upstream of the sample location) (cf. [39]), and may reflect some tectonic control on catchment-wide erosion (cf. [40]).

From the slope of the linear best fit to the E_C–ΔH_{mean} plot (Fig. 5), an erosion time constant, τ, can be calculated, where τ is the time required to lower ΔH_{mean} to 1/e times its initial value. For our data, the slope is ~ 0.1 Myr^{-1}. This implies that in the middle European uplands, $\tau \approx 10$ Myr. Interestingly, this erosion time constant lies between that of 2.5 Myr calculated for active orogens, and that of 25 Myr calculated for tectonically stable areas [38]. This intermediate time constant might

reflect the non-orogenic, Neogene uplift of the middle European uplands.

An important advantage of the cosmogenic nuclide method lies in the long time scales over which the measurements integrate. This enables us to look beyond the complications caused by climate change, land use change, and rapid inflation or deflation of loess. These effects are essentially smoothed out at the 10^4 yr time scale of this method. Therefore, the measured rates capture pre-anthropogenic erosion in a much more accurate manner than previous estimates. Moreover, at the 10^4 yr time scale, bedrock erosion rate will approach the rate of weathering. E_C estimates may therefore reflect the rates of soil formation.

5. Conclusions

The agreement to within less than half an order of magnitude between erosion rate estimates derived from cosmogenic nuclide concentrations in river sands (E_C) and erosion rates calculated from measured solid and dissolved sediment fluxes in rivers (E_G) suggests that the former are reliable at sampling scales of 10^2–10^5 km^2. E_C estimates are relatively uniform within the studied middle European catchments. This demonstrates that the nuclide concentration in well-mixed river sands is governed by the residence of the sediment in the hillslope weathering and mass wasting system, rather than by fluvial transfer.

Cosmogenic nuclide-derived erosion rate estimates are consistently higher than their river load-derived equivalents. Three likely causes for this discrepancy are: (1) systematic underestimation of modern river loads; (2) spatially non-uniform erosion (e.g. linear dissection) and selective tapping of deeper segments of the irradiation profile; and (3) inheritance of a Late Pleistocene erosion signal. At this stage we cannot discount any of these explanations.

The cosmogenic nuclide concentration in an irradiation profile is insensitive to Late Holocene changes in erosion rate. Thus, cosmogenic nuclides can be used to constrain the natural background erosion rate in areas strongly affected by recent changes in land use. Moreover, such nu-

clides allow the evaluation of climatic and tectonic forcing of erosion back through time. In middle Europe, lithology exerts a strong control on erosion. In areas with similar rock mass properties, relief governs erosion. Our data suggest that in the middle European uplands the erosional time constant for reduction of relief is ∼ 10 Myr. Under the assumption that erosion is weathering-limited at the time scale sampled by this method, the cosmogenic nuclide-derived erosion rates are likely to represent bedrock weathering rates.

In conclusion, we propose that, if the complication of sediment storage can be overcome, cosmogenic nuclides offer the opportunity to constrain continental denudation from a limited number of samples from selected large or sediment-laden rivers of the world.

Acknowledgements

References

[1] J.D. Milliman, J.P.M. Syvitski, Geomorphic/tectonic control of sediment discharge to the ocean the importance of small mountainous rivers, J. Geol. 100 (1992) 525–544.

[2] M.A. Summerfield, N.J. Hulton, Natural controls of fluvial denudation rate in major world drainage basins, J. Geophys. Res. 99 (1994) 13871–13883.

[3] J.-J. Macaire, G. Bossuet, A. Choquier, C. Cocirta, P. De Luca, A. Dupis, I. Gay, E. Mathey, P. Guenet, Sediment yield during Late Glacial and Holocene periods in the Lac Chambon watershed, Massif Central, France, Earth Surf. Process. Landforms 22 (1997) 473–489.

[4] M.A. Seidl, W.E. Dietrich, J.W. Kirchner, Longitudinal profile development into bedrock: An analysis of Hawaiian channels, J. Geol. 102 (1994) 457–474.

[5] J.M. Edmond, M.R. Palmer, C.I. Measures, E.T. Brown, Y. Huh, Fluvial geochemistry of the eastern slope of the northeastern Andes and its foredeep in the drainage of the Orinoco in Colombia and Venzuela, Geochim. Cosmochim. Acta 60 (1996) 2949–2976.

[6] J. Gaillardet, B. Dupré, P. Louvat, C.J. Allègre, Global silicate weathering and CO_2 consumption rates deduced from the chemistry of large rivers, Chem. Geol. 159 (1999) 3–30.

[7] D. Lal, B. Peters, Cosmic ray-produced radioactivity on the earth, in: S. Flügge (Ed.), Handbuch der Physik, Springer Verlag, Berlin, 1967, pp. 551–612.

[8] D. Lal, Cosmic ray labeling of erosion surfaces: in situ nuclide production rates and erosion models, Earth Planet. Sci. Lett. 104 (1991) 424–439.

[9] K. Nishiizumi, C.P. Kohl, J.R. Arnold, R. Dorn, J. Klein, D. Fink, R. Middleton, D. Lal, Role of in situ cosmogenic nuclides [10]Be and [26]Al in the study of diverse geomorphic processes, Earth Surf. Process. Landforms 18 (1993) 407–425.

[10] T.E. Cerling, H. Craig, Geomorphology and in-situ cosmogenic isotopes, Annu. Rev. Earth Planet. Sci. 22 (1994) 273–317.

[11] E.T. Brown, R.F. Stallard, M.C. Larsen, G.M. Raisbeck, F. Yiou, Denudation rates determined from the accumulation of in situ-produced [10]Be in the Luquillo Experimental Forest, Puerto Rico, Earth Planet. Sci. Lett. 129 (1995) 193–202.

[12] D.E. Granger, J.W. Kirchner, R. Finkel, Spatially averaged long-term erosion rates measured from in situ-produced cosmogenic nuclides in alluvial sediment, J. Geol. 104 (1996) 249–257.

[13] P. Bierman, E.J. Steig, Estimating rates of denudation using cosmogenic isotope abundances in sediment, Earth Surf. Process. Landforms 21 (1996) 125–139.

[14] C. Grosbois, P. Négrel, C. Fouillac, D. Grimaud, Dissolved load of the Loire River: chemical and isotopic characterization, Chem. Geol. 170 (2000) 179–201.

[15] P. Négrel, C. Grosbois, Changes in chemical and [87]Sr/[86]Sr signature distribution patterns of suspended matter and bed sediments in the upper Loire river basin (France), Chem. Geol. 156 (1999) 231–249.

[16] L.A. Tebbens, Late Quaternary Evolution of the Meuse Fluvial System and its Sediment Composition, Landbouwuniversiteit Wageningen, 1999.

[17] M. Huisink, Lateglacial river sediment budgets in the Maas valley, The Netherlands, Earth Surf. Process. Landforms 12 (1999) 93–109.

[18] F. von Blanckenburg, N.S. Belshaw, R.K. O'Nions, Separation of [9]Be and cosmogenic [10]Be from environmental

materials and SIMS isotope dilution analysis, Chem. Geol. 129 (1996) 93–99.

[19] P.W. Kubik, S. Ivy-Ochs, J. Masarik, M. Frank, C. Schlüchter, ^{10}Be and ^{26}Al production rates deduced from an instantaneous event within the dendro-calibration curve, the landslide of Köfels, Oetz Valley, Austria, Earth Planet. Sci. Lett. 161 (1998) 231–241.

[20] B.P. Heisinger, Myonen-induzierte Produktion von Radionukliden, Technische Universität, Munich, 1998.

[21] J. Masarik, R.C. Reedy, Terrestrial cosmogenic-nuclide production systematics calculated from numerical simulations, Earth Planet. Sci. Lett. 136 (1995) 381–395.

[22] K. Nishiizumi, E.L. Winterer, C.P. Kohl, J. Klein, Cosmic ray production rates of ^{10}Be and ^{26}Al in quartz from glacially polished rocks, J. Geophys. Res. 94 (B12) (1989) 17907–17915.

[23] T.J. Dunai, Scaling factors for production rates of in situ produced cosmogenic nuclides: a critical reevaluation, Earth Planet. Sci. Lett. 176 (2000) 157–169.

[24] J. Masarik, M. Frank, J.M. Schäfer, R. Wieler, 800 kyr calibration of in-situ cosmogenic nuclide production for geomagnetic field intensity variations, Geochim. Cosmochim. Acta (2001) in press.

[25] O.C. Allkofer, Introduction to Cosmic Rays, Verlag Karl Thiemig, Munich, 1975.

[26] E.E. Small, R.S. Anderson, G.S. Hancock, Estimates of the rate of regolith production using ^{10}Be and ^{26}Al from an alpine hillslope, Geomorphology 27 (1999) 131–150.

[27] B.G. Andersen, H.W. Borns Jr., The Ice Age World, Scandinavian University Press, 1994, 208 pp.

[28] A. Henk, F. von Blanckenburg, F. Finger, U. Schaltegger, G. Zulauf, Syn-convergent high-temperature metamorphism and magmatism in the Variscides – a discussion of potential heat sources, Geological Society London Special Publication 179 (2000) 387–399.

[29] M.W. Van den Berg, Fluvial Sequences of the Maas, Landbouwuniversiteit Wageningen, 1996.

[30] J.P. Larue, Les nappes alluviales de la Loire et de ses affluents dans le Massif Central et dans le Sud de bassin Parisien: étude géomorphologique, Univ. Clermont II, 1979.

[31] J.F. Pastre, Altération et paleoaltération des minéraux lourds des alluvions Pliocènes et Pleistocènes du bassin de l'Allier (Massif Central, France), Assoc. Rf. Etude Quat. Bull. 3/4 (1986) 257–269.

[32] H.-R. Bork, H. Bork, C. Dalchow, B. Faust, H.-P. Piorr, T. Schatz, Landschaftsentwicklung in Mitteleuropa, Klett-Perthes, Gotha, 1998, 328 pp.

[33] A. Goudie, The Changing Earth, Blackwell, Oxford, 1995, 302 pp.

[34] A. Galy, C. France-Lanord, Higher erosion rates in the Himalaya: Geochemical constraints on riverine fluxes, Geology 29 (2001) 23–26.

[35] I. Saunders, A. Young, Rates of surface processes on slopes, slope retreat and denudation, Earth Surf. Process. Landforms 8 (1983) 473–501.

[36] P.R. Bierman, Using in situ produced isotopes to estimate rates of landscape evolution: a review from the geomorphic perspective, J. Geophys. Res. 99 (1994) 13885–13896.

[37] B. Frenzel, European river activity and climatic change during the Lateglacial and early Holocene, in: Palaeoclimate Research 14, Akademie der Wissenschaften und der Literatur, Mainz, 1995, p. 222.

[38] P. Pinet, M. Souriau, Continental erosion and large-scale relief, Tectonics 7 (1988) 563–582.

[39] F. Ahnert, Functional relationships between denudation, relief, and uplift in large mid-latitude drainage basins, Am. J. Sci. 268 (1970) 243–263.

[40] C.S. Riebe, J.W. Kirchner, D.E. Granger, R.C. Finkel, Erosional equilibrium and disequilibrium in the Sierra Nevada, inferred from cosmogenic ^{26}Al and ^{10}Be in alluvial sediment, Geology 28 (2000) 803–806.

[41] H. Walter, H. Lieth, Klimadiagramm-Weltatlas, VEB Gustav Fischer Verlag, Jena, 1967.

[42] World Atlas of Agriculture 1, Istituto de Agostini, Novara, 1969.

[43] R. Hantke, Flussgeschichte Mitteleuropas, Ferdinand Enke Verlag, Stuttgart, 1993, 459 pp.

[44] K. Rother, Die eiszeitliche Vergletscherung der deutschen Mittelgebirge im Spiegel neuerer Forschungen, Petermanns Geogr. Mitt. 139 (1995) 45–52.

[45] Y. Veyret, Quaternary glaciations in the French Massif Central, in: V. Sibrava, D.Q. Bowen, G.M. Richmond (Eds.), Quaternary Glaciation in the Northern Hemisphere, International Union of Geological Sciences and UNESCO, Geneva, 1986, 513 pp.

[46] K. Zippelt, H. Mälzer, Recent height changes in the central segment of the Rhinegraben and its adjacent shoulders, Tectonophysics 73 (1981) 119–123.

[47] M.W. Van den Berg, Neotectonics of the Roer Valley rift system. Style and rate of crustal deformation inferred from syn-tectonic sedimentation, Geol. Mijnb. 73 (1994) 143–156.

[48] A. Veldkamp, Quaternary River Terrace Formation in the Allier Basin, France, Landbouwuniversiteit Wageningen, 1991.

[49] M.A. Summerfield, Global Geomorphology, Longman, London, 1991, 537 pp.

[50] E.K. Berner, R.A. Berner, The Global Water Cycle, Prentice-Hall, New York, 1987, 397 pp.

[51] K. Kille, Das Verfahren MoMNQ, ein Beitrag zur Berechnung der mittleren langjährigen Grundwasserneubildung mit Hilfe der monatlichen Niedrigwasserabflüsse, Z. Dtsch. Geol. Ges. Sonderh. Hydrogeol. Hydrogeochem. (1970) 89–95.

[52] D. Barsch, R. Mäusbacher, G. Schukraft, A. Schulte, Hochwasserdynamik und Sedimenttransport, in: D. Barsch, R. Mäusbacher, K.-H. Pörtge, K.-H. Schmidt (Eds.), Messungen in fluvialen Systemen, Springer Verlag, Berlin, 1994, pp. 71–100.